

# **Inductor Design with Emphasis on Inductance Calculation**

A project report (Course code: EE699 ) submitted in partial fulfillment of  
the requirements for the degree of

**Master of Technology**

by

**Peace Panmei**  
**(Entry No. 2023EEM1020)**

Under the guidance of  
**Prof.Mahendra Sakare**



**DEPARTMENT OF ELECTRICAL ENGINEERING**  
**INDIAN INSTITUTE OF TECHNOLOGY ROPAR**  
**2024**

# **Declaration**

I hereby, declare that this written submission titled, "Inductor Design with Emphasis on Inductance Calculation" contains my research works and has been completed with adequate citations and references to the original sources. I also declare that no falsified interpretation has been done and I have adhered to all the ethics and principles of academic integrity. Further, if any violation of the aforementioned statement is found I will be held responsible and I fully understand the consequences.

---

Peace Panmei  
Entry No. 2023EEM1020

Date:22/11/2024

# **Acknowledgment**

I would like to convey my utmost gratitude and sincere thanks towards my supervisor Dr. Mahendra Sakare for providing me the opportunity to study and work in this Master Thesis Project (phase-1). I would like to extend my heart-felt appreciation for the determination and help in this project. I would also like to acknowledge and extend my heartfelt gratitude to my senior research members of VLSI lab for their unending support and valuable suggestions in the ongoing project work. And I extend my heartfelt gratitude towards IIT Ropar and also the Ministry of Education for their role in providing the platform for the project.

---

Peace Panmei

Entry No. 2023EEM1020

Date:22/11/2024

# Abstract

This report contains the design of an inductor by deriving expressions to calculate the inductance provided by a particular geometrical shape. Different methods of calculation for inductance has also been studied in the literature review. An approximation of current sheet has been done in this work to calculate the inductance. The sheet approximation is entirely based on approximation of distances mainly the Geometric mean distance (GMD), Arithmetic mean distance (AMD) and Arithmetic mean square distance (ASMD). A Skill coding based on parameterized cell has been used to automatically generate the layout of the inductor in cadence and EMX simulation was done to find how the inductor work with respect to changing frequency. The shape generated in the layout has been taken into consideration while calculating the inductance theoretically with the current sheet approximation method and has been verified by EMX simulation. The designed inductor is then integrated into a complimentary Inductance Capacitance based Voltage Controlled Oscillator (LC-VCO) to test various parameters including phase noise and figure of merits (FOMs) at various frequencies. Post layout simulations for transient response reveal a voltage swing of about 700 mV and also a phase noise of -97 dBc/Hz and -118 dBc/Hz at 100 KHz and 1 MHz respectively has been detected. The power consumption of the VCO is 5.96 at 4.6 GHz frequency of oscillation and the the inductor has a quality factor of around 13 at the same frequency. All simulations are done in TSMC 65 nm technology.

# Contents

<b>Abstract</b>	<b>i</b>
<b>List of Tables</b>	<b>iv</b>
<b>List of Figures</b>	<b>v</b>
<b>1 Introduction</b>	<b>1</b>
<b>2 Literature survey</b>	<b>3</b>
<b>3 Realization of on-chip planar spiral Inductor and its modeling</b>	<b>7</b>
3.1 Structure of on-chip inductor . . . . .	7
3.2 Derivation of Inductance equation . . . . .	10
3.2.1 Neuman Equation . . . . .	10
3.2.2 Self-inductance of a trapezoidal current sheet . . . . .	12
3.2.3 Mutual inductance of two parallel trapezoidal sheets . . . . .	16
3.2.4 Approximation for a family of trapezoid sheets . . . . .	18
3.3 Modeling of inductor . . . . .	20
3.3.1 Derivation of series resistance . . . . .	21
3.4 Quality factor of inductor . . . . .	22
<b>4 Theoretical verification and simulation results</b>	<b>24</b>
4.1 Theoretical calculation of the inductor under consideration . . . . .	24
4.1.1 VCO implementation . . . . .	26
4.2 Simulation Results . . . . .	27
4.2.1 EMX simulations . . . . .	27
4.2.2 Post Layout simulation results . . . . .	28

4.3 Comparison . . . . .	31
<b>5 Conclusion and future works</b>	<b>32</b>

# List of Tables

4.1	Specification of the designed LC-VCO . . . . .	30
4.2	Comparison table of different formulas . . . . .	31
4.3	Comparison table for different architectures of LC-VCO . . . . .	31

# List of Figures

2.1	Different types of planar spiral inductor structures . . . . .	4
3.1	Square spiral . . . . .	8
3.2	Hexagonal spiral . . . . .	8
3.3	Octagonal spiral . . . . .	8
3.4	A spiral inductor as seen from the front . . . . .	9
3.5	Two parallel lines with their center aligned . . . . .	10
3.6	A trapezoidal current sheet . . . . .	12
3.7	Parallel trapezoidal current sheet . . . . .	16
3.8	A square spiral inductor . . . . .	18
3.9	(a) Concentric squares and (b) approximated trapezoids . . . . .	19
3.10	Lumped/Pi model of inductor . . . . .	20
3.11	A 3-D view of a wire strip with visible skin effect . . . . .	22
3.12	Modified form of the inductor model in figure 3.10 . . . . .	23
4.1	Layout view of the inductor under consideration . . . . .	25
4.2	A complimentary LC-VCO circuit diagram . . . . .	26
4.3	(a) Layout view of LC-VCO and (b) Zoomed-in view of the LC-VCO . . . . .	27
4.4	(a) Inductance vs frequency and (b) Quality factor vs frequency . . . . .	27
4.5	(a) Voltage swing of the LC-VCO and (b) Phase Noise of the LC-VCO . . . . .	28
4.6	Variation of frequency for temperature change from $-20^{\circ}\text{C}$ to $127^{\circ}\text{C}$ and for sensitivity of supply voltage from 0.9 V to 1.1V . . . . .	28
4.7	(a) to (h ) shows individual points of the PVT simulations from figure 4.6 . . . . .	29

4.8 Monte Carlo simulation results for mismatch and process variation of (a) Frequency, (b) Power consumption, (c) Phase noise @ 100 KHz, and (d) Phase noise @ 1 MHz . . . . .	30
---	----

# Chapter 1

## Introduction

Apart from conventional analog circuits, modern high-frequency circuits require extra passive devices, especially inductors and transformers. These devices need to be integrated into a single chip and need to be optimized for better performance and smaller chip area. Given the bulky size of an inductor, designers generally keep inductors off-chip for better integration of other components. However, the advancement in CMOS technology allows inductors to be integrated inside the chip resulting in smaller cheap area and also reducing power consumption. This optimization leads to cheaper cost of the circuits facilitating easier commercial production.

Inductors are also used in LC-based Voltage Controlled Oscillators which is an important part in Phase Locked Loop. And phase noise, being an inherent part of PLL though unwanted, affects optimal locking at the targeted frequency. Oscillators that are designed with active elements, for example, a ring VCO produce a substantial contribution to phase noise. Therefore, to minimize phase noise, designers move towards an integrated inductor, meaning an on-chip inductor to be used in LC-based oscillators.

Though inductors provide a relatively lower phase noise as compared to their equivalent counterparts, the area occupancy and the power consumption act as the main trade-offs in LC-based circuits. And optimization of inductors requires time and rigor analysis. For these reasons, many researchers have developed some highly accurate expressions to analyze the behavior of an inductor and predict its inductance with the help of such formulas and expressions. Even though such formulas exist, the complexity in their computation often hinders progress at the initial stages of inductor design. This work explores derivations and the resulting expressions as a function of their geometrical properties at the same time, simple enough for quick analysis in the design of inductors.

The thesis is organized into multiple chapters with Chapter 1 as the introduction followed by Chapter 2 with a literature survey. Then, the research work containing the derivation of formulas is Chapter 3 followed by the design of a square-shaped inductor. The theoretical derivation is verified in Chapter 4 and the designed inductor is applied in an LC-VCO followed by simulation results and comparisons.

In the next chapter, we shall look into the works of various researchers and explore in detail the past scientific research works on inductor design, its modeling, and the implementations of inductors in radio frequency circuits.

# Chapter 2

## Literature survey

In modern Radio Frequency circuits, inductors have one of the most crucial role in determining the speed and performance. With the increasing demands for small-area circuits, circuits with active inductor implementation are also developed. Even though such circuits occupy less area, a passive inductor have an extra edge as per noise and power consumption. Such passive inductors are also referred to as on-chip inductors as they are integrated along with the other components in the IC. The most frequently used type of on-chip inductor is the planar spiral and the realization of on-chip inductors are done using multiple metal layers placed on top of a silicon substrate. It can take different shapes based on requirements and fabrication capability. Different structures of an inductors are shown in figure 2.1. The inductance and the quality factor provided by these inductors depends on their geometrical structures. The Quality factor determine the series resistance and the loss in magnetic energy due to the inherent parasitics and its interaction with the substrate.

Significant research has been carried out to find an expression for finding the inductance using its parameters like the width, the spacing in between, and the diameter of the structure involved. Many formulas were developed by various researchers to predict the behavior of inductor with a given shape. One of the earlier works on inductance is given by H.A Wheeler based on the geometrical shape of the inductor and one such modified form of the formula is given in [1].

$$L = K_1 \mu_0 \frac{n^2 d_{avg}}{1 + K_2 \rho}$$

where  $\rho$  is the fill ratio,  $d_{avg}$  is the arithmetic mean of the inner diameter of the inductor structure and the outer diameter of the inductor structure and can be seen in figure 2.1 and the coefficients are  $K_1$  and  $K_2$  depends on the layout.

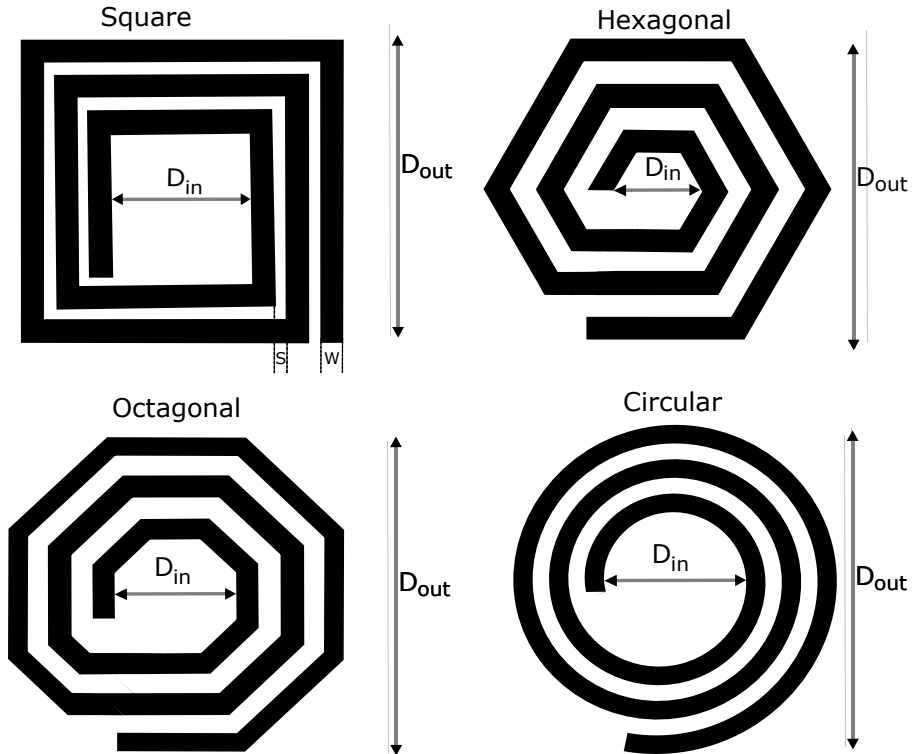


Figure 2.1: Different types of planar spiral inductor structures

A few other methods for inductance calculation are given by H.M. Greenhouse in his paper [2] which explore different methods namely Grover method [3] based on geometric mean distance. Snezana's paper [4] also gives a physics-based inductance expression in closed form. This work allows compact modeling and is based on decomposing the inductor segments and averaging the segments. Due to its physics-based nature. A formula is also given in [5] defined in terms of the spiral's geometry. The empirical formula is

$$L \approx 1.3 \times 10^{-7} \frac{A_m^{5/3}}{A_{tot}^{1/6} W^{1.75} (W + S)^{0.25}}$$

where  $A_m$  is the area of the metal strip and  $A_{tot}$  is the area occupied by the whole structure of the inductor geometry. A method based on current sheet approximation is also given in [6] which approximated the inductance by approximation of symmetrical current sheets. The inductance calculation is built upon the concept of geometric mean and the arithmetic mean of distances. [1] also gives a formula based on data fitting and the expression is given by,

$$L = \beta d_{out}^{a_1} w^{a_2} d_{avg}^{a_3} n^{a_4} s^{a_5}$$

where  $\beta$  and  $a_i$  depend on layout. This simple expression employs data fitting techniques by fitting approximately 19000 inductors.

Different architectures of inductors are also explored to better optimize them for application in circuits such as LC-Voltage Controlled Oscillators. The expression given by these literatures from [1] to [5] based on their geometrical properties are applicable for simple structures. But when shapes with complex geometries are involved, the formulas and expressions prove rather invalid as these formulas are based on simple structures. For inductor structures with higher geometrical complexities, different modeling is also developed for predicting the behavior of such complex structures.

Yue's paper [7] presented a physical model for spiral inductor with a planar structure and also presented a method to predict the behavior of a spiral shaped on-chip inductor. The model is also known as the Pi-model/ lumped model and also the literature considers various parameters other than inductance to determine how the inductor behave w.r.t frequency change. The lumped model gives an accurate representation of the electrical behavior of an inductor. B. Kuhn also presented a model in his paper [8]. He developed a frequency-independent expression for four-elements and five-elements model with comparison to measured results. When compared with the Pi model, certain similarities like accounting for the effective reduction in Q, and dissimilarities like ground connection in the two models are presented.

Crols in his paper [9] also developed an model based on analytical results that can be used for planar spiral inductors. He claims his model produces more accuracy than 10 percent of various inductor geometries. Even properties like the metal line spacing are taken into account. This paper also provides the relationship between layout parameters and electrical parameters. An efficient modeling is also presented by Yorgos in his paper [10]. He established a connection with measurements of various inductor which are already fabricated. Yorgos's model is also applicable to both spiral inductors and transformers. Also for center-tap inductors, Tian [11] presents a characteristic approach to parameter extraction and develops a closed-form analytical expression for a center-tap branch. The analytical method is verified by high-precision simulations for  $0.18 \mu m$  fabricated center-tap inductor. The paper is based on measured S-parameter extraction and also through a set of Y and Z parameters.

Darabi in his book [12] presented an expression for inductance by relating it with the frequency dependence of L (inductance). The pi-model was used to derive an expression for inductance. All other dependencies on the substrate are also included in this expression.

$$L(\omega) \approx L \frac{1 - LC_{\text{sub}}\omega^2}{(1 - LC_{\text{sub}}\omega^2)^2 + \left[ \left( \frac{L}{R_{\text{sub}} + rC_{\text{sub}}} \right) \omega \right]^2}$$

This expression also accounts for self-resonant frequency and is evident that the  $L(\omega)$  approaches zero at self-resonant frequency (SRF) and becomes capacitive thereafter.

Apart from the different inductor models, studies have been done on more complex structures of inductors and how their geometry affects the inductances and other interactive parameters. Apart from the conventional structures, new geometries with a higher symmetry are also studied to explore their interaction and the crosstalk with other circuit elements in the proximity of the inductor. The symmetric shape provides better performance as proven and cited in [13]. This is due to a lesser number of overlaps and shorter underpasses which in turn decreases capacitance thereby improving the quality factor. The conventional structure including the square and the hexagonal structure are modified for symmetry and improved results in terms of Quality factor and phase noise. Even the chip area is reduced as claimed by [14] as these symmetric structures occupy lesser space as compared to their asymmetric counterparts. Stacked structures also known as transformers are inductors with multiple spirals stacked together. Design and analysis of such planar transformer is reported in Niknejad's paper [15] and he extensively studied and has done detailed analysis on transformers and presents simulations and measured results. Several techniques were also provided by the paper for analysis and modeling of spiral inductors for better optimization. A honeycomb shape structure was also studied as given in [16]. The paper reported a new planar inductor layout in the shape of a honeycomb. This shape suppressed interferences or crosstalk between the inductor and other circuit components. The achieved suppression is due to the opposite magnetic dipoles which cancel out the EMI emissions. The coils are also area-efficient as it is based on honeycombs which are considered one of the most compact structures in nature.

A PCell design methodology using SKILL scripting language was studied as given in [17]. The algorithms provided in the paper allows the user to create a cell by the use of SKILL commands to create polygons that can further be designed into spiral inductor shapes. Sample scripting codes are also presented in [18] and flowcharts are provided for the design procedure of different inductors in PCell Design Methodology.

The next chapter further dives into the design of the inductor and its relationship with its geometrical properties through mathematical expressions and will reveal how the physical properties can be utilized to control the performance of an inductor.

# **Chapter 3**

## **Realization of on-chip planar spiral Inductor and its modeling**

On-chip inductors are an essential part of every RF Circuit especially when LC-based Voltage Controlled Oscillators are involved. Such inductors are integrated along with other components in a single chip area, hence the name on-chip. This integration allows a lesser number of external connections and increases robustness. The chapter is organized into sub-parts starting from defining the parameters of an on-chip inductor to finding an expression that is simple enough and can predict the behavior of the inductor followed by modeling.

### **3.1 Structure of on-chip inductor**

Some common forms of inductors are the square, hexagonal and the octagonal shape inductor, and the different types of square inductors are shown in the subsequent figures. The inductance of an inductor is wound tightly with its geometrical properties. Attributes like the number of turns of the spiral, the width of metal strip, and the spacing between the strips play a crucial role in determining the behavior of an inductor. Even the inner and the outer diameter are important factors in its performance. A circular shape inductor provides the best quality factor but fabrication restrains such shapes. And though a square-shaped inductor is easily fabricated, sharp corners in the design create a higher series resistance. Therefore a square shape which is easy to build can be modified by increasing its sides to realize a hexagonal or an octagonal-shaped inductor.

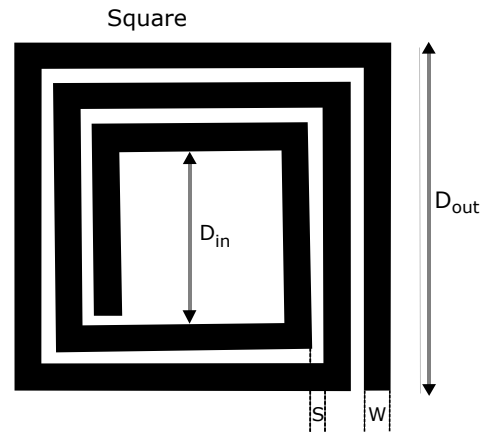


Figure 3.1: Square spiral

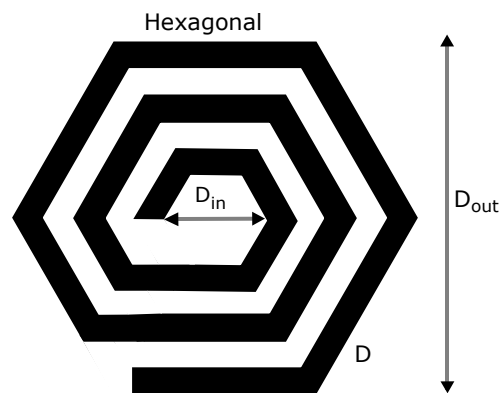


Figure 3.2: Hexagonal spiral

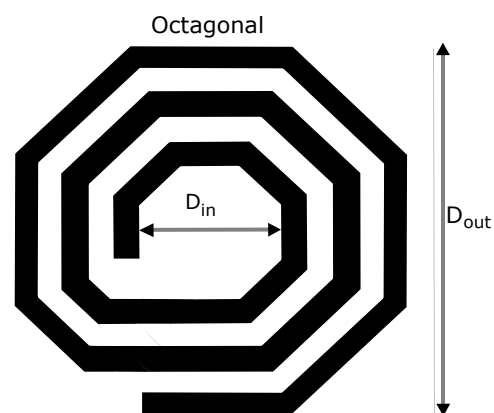


Figure 3.3: Octagonal spiral

The most important parameters that must be considered while designing an inductor are the number of turns  $n$ , the width of the metal trace  $w$ , the space between the metal traces  $s$ , and the inner diameter  $D_{in}$  and the outer diameter  $D_{out}$ . The description is shown figuratively in figure 3.1 in the square spiral shape with all the defined parameters. The average diameter is also sometimes used and is given by  $D_{avg} = \frac{1}{2} \times (D_{out} - D_{in})$ . A front view of the spiral inductor is also shown in figure 3.4

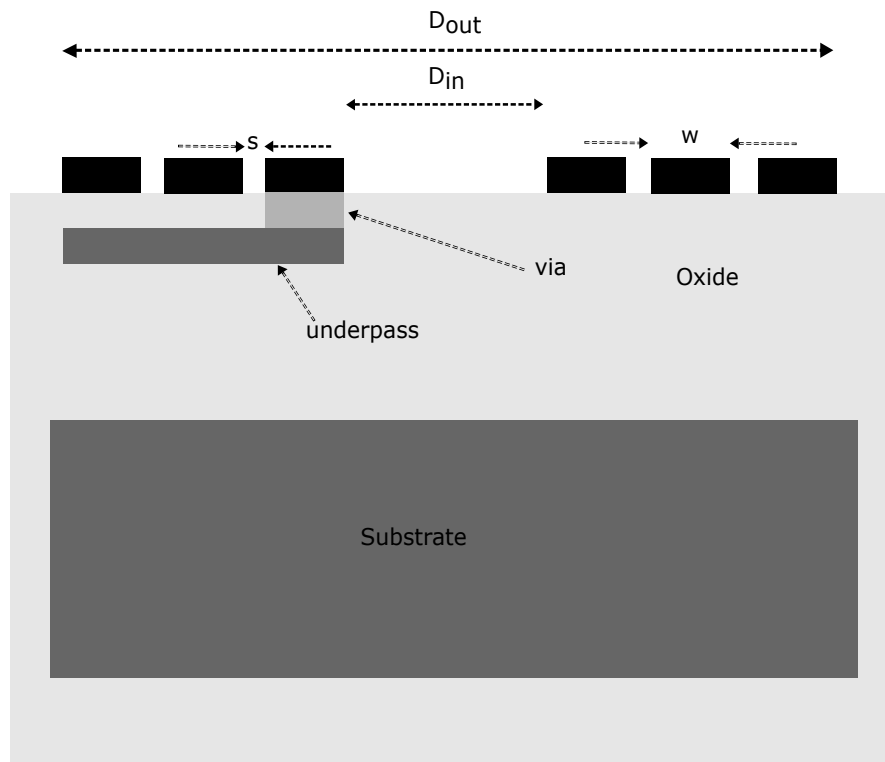


Figure 3.4: A spiral inductor as seen from the front

The vertical representation of the on-chip inductor reveals how the metals are arranged in the chip. Thicker metals(usually metal 9) are used as the material for the spiral in order to facilitate a lower resistance path to the current. The underpass as seen in figure 3.4 is the main contributor to the capacitive loss of the inductor thus affecting the quality factor negatively. The total inductance offered by the full spiral is calculated by summing up the self-inductances and the mutual inductances of the different segments of the inductor. The number of turns  $n$ , also determine the total inductance offered by a particular inductor.

## 3.2 Derivation of Inductance equation

The mathematical relations between the inductor attributes and the inductance are derived in this section. We derive the mutual inductance between two straight lines and extend the concept to sheet metals using approximations described in the later part of the chapter.

### 3.2.1 Neuman Equation

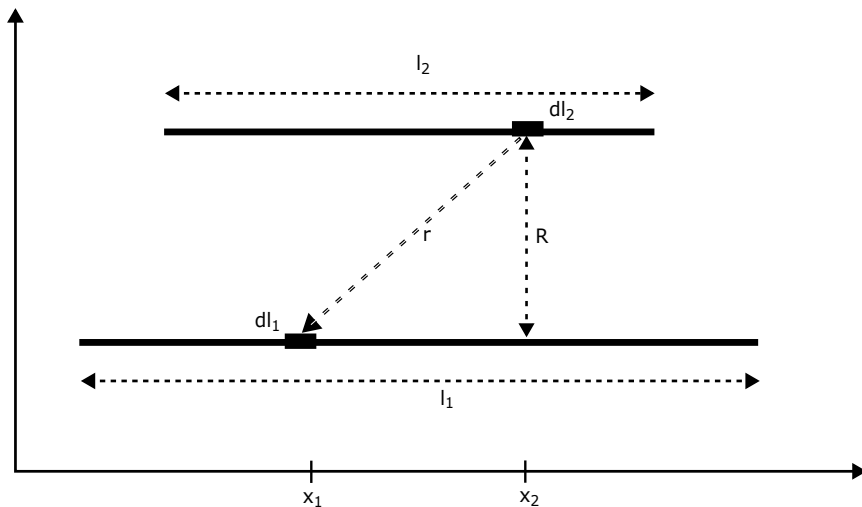


Figure 3.5: Two parallel lines with their center alligned

The Neuman integral for two unequal lines is given by,

$$M = \frac{\mu}{4\pi} \oint \oint \frac{1}{r} dl_1 \cdot dl_2 \quad (3.1)$$

Here, the center of the two lines are aligned and an infinitesimal element,  $dl_1$  and  $dl_2$  are defined on line  $l_1$  and  $l_2$ . The perpendicular distance between the two lines is  $R$  and the distance between the two arbitrary infinitesimal elements is  $r$ .

$$\begin{aligned} M &= \frac{\mu}{4\pi} \oint \oint \frac{1}{r} dl_1 \cdot dl_2 \\ &= \frac{\mu}{4\pi} \oint \oint \frac{dx_1 dx_2}{R^2 + (x_1 - x_2)^2} \end{aligned}$$

Putting limits,

$$= \frac{\mu}{4\pi} \int_{-\frac{l_1}{2}}^{\frac{l_1}{2}} \int_{-\frac{l_2}{2}}^{\frac{l_2}{2}} \frac{dx_1 dx_2}{R^2 + (x_1 - x_2)^2}$$

Let  $u = x_1 - x_2$ , then  $du = dx_1$

Thus, the integral is

$$\begin{aligned}
M &= \frac{\mu}{4\pi} \int_{-\frac{l_1}{2}}^{\frac{l_1}{2}} \int_{-\frac{l_2}{2}}^{\frac{l_2}{2}} \frac{du}{\sqrt{R^2 + u^2}} dx_2 \\
&= \frac{\mu}{4\pi} \int_{-\frac{l_2}{2}}^{\frac{l_2}{2}} \left[ \ln \left( \left( \frac{l_1}{2} - x_2 \right) + \sqrt{R^2 + \left( \frac{l_1}{2} - x_2 \right)^2} \right) \right] dx_2 \\
&\quad - \left[ \ln \left( \left( \frac{-l_1}{2} - x_2 \right) + \sqrt{R^2 + \left( \frac{-l_1}{2} - x_2 \right)^2} \right) \right] dx_2
\end{aligned}$$

Applying limits,

$$\begin{aligned}
M &= \frac{\mu}{4\pi} \left( \frac{l_1 + l_2}{2} \right) \left[ \ln \left( \left( \frac{l_1 + l_2}{2} \right) + \sqrt{R^2 + \left( \frac{l_1 + l_2}{2} \right)^2} \right) \right. \\
&\quad \left. - \ln \left( \left( \frac{l_1 + l_2}{2} \right) + \sqrt{R^2 + \left( \frac{l_1 + l_2}{2} \right)^2} \right) \right] \\
&\quad - \frac{\mu}{4\pi} \left( \frac{l_1 - l_2}{2} \right) \left[ \ln \left( \left( \frac{l_1 - l_2}{2} \right) + \sqrt{R^2 + \left( \frac{l_1 - l_2}{2} \right)^2} \right) \right. \\
&\quad \left. - \ln \left( \left( \frac{l_1 - l_2}{2} \right) + \sqrt{R^2 + \left( \frac{l_1 - l_2}{2} \right)^2} \right) \right] \\
&\quad + \frac{\mu}{2\pi} \sqrt{R^2 + \left( \frac{l_1 - l_2}{2} \right)^2} - \frac{\mu}{2\pi} \sqrt{R^2 + \left( \frac{l_1 + l_2}{2} \right)^2}
\end{aligned}$$

$$\begin{aligned}
M &= \frac{\mu}{2\pi} \left( \frac{l_1 + l_2}{2} \right) \ln \left( \frac{\frac{l_1 + l_2}{2} + \sqrt{R^2 + \left( \frac{l_1 + l_2}{2} \right)^2}}{R} \right) \\
&\quad - \frac{\mu}{2\pi} \left( \frac{l_1 - l_2}{2} \right) \ln \left( \frac{\frac{l_1 - l_2}{2} + \sqrt{R^2 + \left( \frac{l_1 - l_2}{2} \right)^2}}{R} \right) \\
&\quad + \frac{\mu}{2\pi} \sqrt{R^2 + \left( \frac{l_1 - l_2}{2} \right)^2} - \frac{\mu}{2\pi} \sqrt{R^2 + \left( \frac{l_1 + l_2}{2} \right)^2}
\end{aligned}$$

Therefore the closed form solution of equation (3.1) is,

$$M = \frac{\mu}{2\pi} \left[ \left( \frac{l_1 + l_2}{2} \right) \ln \left( \sqrt{\left( \frac{l_1 + l_2}{2R} \right)^2 + 1} + \left( \frac{l_1 + l_2}{2} \right) \right) - \sqrt{\left( \frac{l_1 + l_2}{2} \right)^2 + R^2} \right] - \frac{\mu}{2\pi} \left[ \left( \frac{l_1 - l_2}{2} \right) \ln \left( \sqrt{\left( \frac{l_1 - l_2}{2R} \right)^2 + 1} + \left( \frac{l_1 - l_2}{2} \right) \right) - \sqrt{\left( \frac{l_1 - l_2}{2} \right)^2 + R^2} \right] \quad (3.2)$$

Equation (3.2) gives the total mutual inductance between two unequal parallel lines and the results will also be used in the later part of the chapter.

### 3.2.2 Self-inductance of a trapezoidal current sheet

A current sheet is a metal sheet whose thickness is infinitesimally small and with a finite thickness. Though not physically possible, the concept of current sheet is sufficient for certain calculations when the metal thickness is very small. We consider a current sheet 3.6 which is trapezoidal in shape and has a current  $I$  flowing through it. Consider two lines  $l_1$  and  $l_2$  in the current sheet. Here,  $l$  is the length of the trapezoid at the middle of the shape,  $l_1$  is at  $x_1$  and  $l_2$  is at  $x_2$ . The mutual inductance equation (3.2) is used to derive the equation for mutual inductance between the two filaments that was considered inside the trapezoidal current sheet. Here,  $R = x_1 - x_2$ ,  $l_1 = l + 2x_1$  and  $l_2 = l + 2x_2$

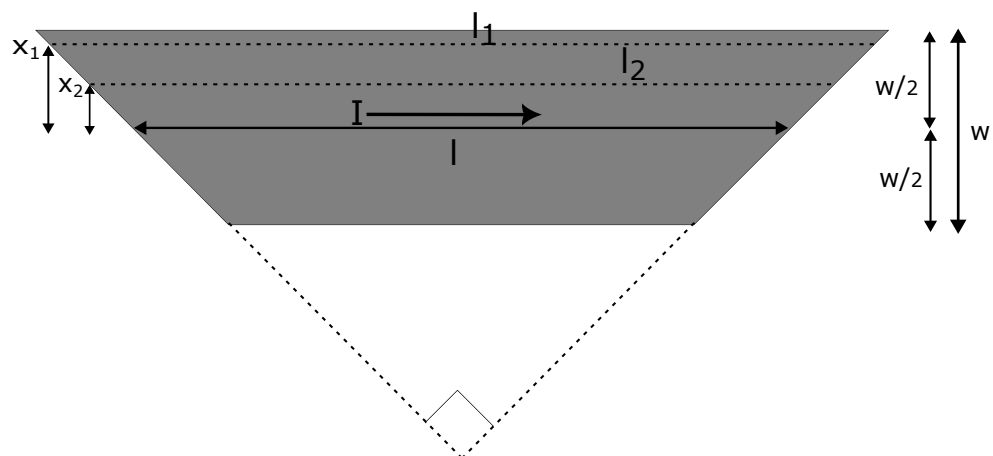


Figure 3.6: A trapezoidal current sheet

Substituting the values of  $x_1$  and  $x_2$  in equation 3.2,

$$\begin{aligned}
M &= \frac{\mu}{2\pi} \left[ \left( \frac{l_1 + l_2}{2} \right) \ln \left( \sqrt{\left( \frac{l_1 + l_2}{2R} \right)^2 + 1} + \left( \frac{l_1 + l_2}{2} \right) \right) - \sqrt{\left( \frac{l_1 + l_2}{2} \right)^2 + R^2} \right] \\
&\quad - \frac{\mu}{2\pi} \left[ \left( \frac{l_1 - l_2}{2} \right) \ln \left( \sqrt{\left( \frac{l_1 - l_2}{2R} \right)^2 + 1} + \left( \frac{l_1 - l_2}{2} \right) \right) - \sqrt{\left( \frac{l_1 - l_2}{2} \right)^2 + R^2} \right] \\
&= \frac{\mu}{2\pi} \left[ \left( \frac{l_1 + l_2}{2} \right) \ln \left( \frac{l_1 + l_2}{2R} \sqrt{1 + \left( \frac{2R}{l_1 + l_2} \right)^2} + \left( \frac{l_1 + l_2}{2R} \right) \right) - \sqrt{\left( \frac{l_1 + l_2}{2} \right)^2 + R^2} \right] \\
&\quad - \frac{\mu}{2\pi} \left[ R \ln((\sqrt{2} + 1) - \sqrt{2}) \right]
\end{aligned}$$

Using series expansion,

$$\begin{aligned}
&= \frac{\mu}{2\pi} \left[ \left( \frac{l_1 + l_2}{2} \right) \ln \left( \frac{l_1 + l_2}{R} \left( 1 + \left( \frac{R}{l_1 + l_2} \right)^2 \right) \right) - \sqrt{\left( \frac{l_1 + l_2}{2} \right)^2 + R^2} \right] \\
&\quad - \frac{\mu}{2\pi} \left[ R \ln(\sqrt{2} + 1 - \sqrt{2}) \right] \\
&= \frac{\mu}{2\pi} \left[ \left( \frac{l_1 + l_2}{2} \right) \left( \ln(l_1 + l_2) + \ln \left( 1 + \left( \frac{R}{l_1 + l_2} \right)^2 \right) - \ln R \right) - \sqrt{\left( \frac{l_1 + l_2}{2} \right)^2 + R^2} \right] \\
&\quad - \frac{\mu}{2\pi} \left[ R \ln(\sqrt{2} + 1 - \sqrt{2}) \right] \\
&= \frac{\mu}{2\pi} \left[ \left( \frac{l_1 + l_2}{2} \right) \left( \ln(l_1 + l_2) + \left( \frac{R}{l_1 + l_2} \right)^2 - \ln R \right) - \sqrt{\left( \frac{l_1 + l_2}{2} \right)^2 + R^2} \right] \\
&\quad - \frac{\mu}{2\pi} \left[ R \ln(\sqrt{2} + 1 - \sqrt{2}) \right] \\
&= \frac{\mu}{2\pi} \left[ \left( \frac{l_1 + l_2}{2} \right) \left( \ln(2l + 2(x_1 + x_2)) + \left( \frac{R}{l_1 + l_2} \right)^2 - \ln R \right) - \sqrt{\left( \frac{l_1 + l_2}{2} \right)^2 + R^2} \right] \\
&\quad - \frac{\mu}{2\pi} \left[ R \ln(\sqrt{2} + 1 - \sqrt{2}) \right]
\end{aligned}$$

$$\begin{aligned}
&= \frac{\mu}{2\pi} \left[ \left( \frac{l_1 + l_2}{2} \right) \left( \ln 2l \left( 1 + \frac{(x_1 + x_2)}{1} \right) + \left( \frac{R}{l_1 + l_2} \right)^2 - \ln R \right) - \sqrt{\left( \frac{l_1 + l_2}{2} \right)^2 + R^2} \right] \\
&\quad - \frac{\mu}{2\pi} \left[ R \ln(\sqrt{2} + 1 - \sqrt{2}) \right] \\
&= \frac{\mu}{2\pi} \left[ \left( \frac{l_1 + l_2}{2} \right) \left( \ln 2l \left( 1 + \frac{(x_1 + x_2)}{1} \right) + \left( \frac{R}{l_1 + l_2} \right)^2 - \ln R \right) - \left( \frac{l_1 + l_2}{2} \right) \left( 1 + 2 \left( \frac{R}{l_1 + l_2} \right)^2 \right) \right] \\
&\quad - \frac{\mu}{2\pi} \left[ R \ln(\sqrt{2} + 1 - \sqrt{2}) \right] \\
&= \frac{\mu}{2\pi} \left[ \left( \frac{l_1 + l_2}{2} \right) \left( \ln 2l + \frac{(x_1 + x_2)}{1} + \left( \frac{R}{l_1 + l_2} \right)^2 - \ln R \right) - \left( \frac{l_1 + l_2}{2} \right) \left( 1 + 2 \left( \frac{R}{l_1 + l_2} \right)^2 \right) \right] \\
&\quad - \frac{\mu}{2\pi} \left[ R \ln(\sqrt{2} + 1 - \sqrt{2}) \right] \\
&= \frac{\mu}{2\pi} \left[ l \ln 2l - l \ln R + (x_1 + x_2) + \left( \frac{R}{l_1 + l_2} \right)^2 l + (x_1 + x_2) \ln 2l + \frac{(x_1 + x_2)^2}{1} \right. \\
&\quad \left. + (x_1 + x_2) \left( \frac{R}{l_1 + l_2} \right)^2 - (x_1 + x_2) \ln R - \frac{l_1 + l_2}{2} - \frac{R^2}{l_1 + l_2} \right] \\
&\quad - \frac{\mu}{2\pi} \left[ R \ln(\sqrt{2} + 1 - \sqrt{2}) \right] \\
&= \frac{\mu}{2\pi} \left[ l \ln 2l - l \ln(x_1 - x_2) + (x_1 + x_2) + \left( \frac{x_1 - x_2}{l_1 + l_2} \right)^2 l + (x_1 + x_2) \ln 2l \right. \\
&\quad \left. + \frac{(x_1 + x_2)^2}{1} + (x_1 + x_2) \left( \frac{x_1 - x_2}{l_1 + l_2} \right)^2 - (x_1 + x_2) \ln(x_1 - x_2) - \frac{l_1 + l_2}{2} \right. \\
&\quad \left. - \frac{(x_1 - x_2)^2}{l_1 + l_2} - (x_1 - x_2) \ln(\sqrt{2} + 1 - \sqrt{2}) \right] \\
M &\approx \frac{\mu l}{2\pi} \left[ \ln 2l - \ln |x_1 - (x_2)| - \frac{|x_1 - x_2| (\ln(\sqrt{2} + 1) - \sqrt{2})}{1} \right] \\
&\quad + \frac{\mu l}{2\pi} \left[ \frac{(x_1 + x_2)^2}{2l^2} - \frac{(x_1 - x_2)^2}{4l^2} \right]
\end{aligned}$$

For determining the self-inductance of the entirety of the trapezoidal current sheet, several averaging techniques including geometric mean distance(GMD), arithmetic mean distance(AMD), and arithmetic mean square distance(AMSD) as given in [6] was utilized and they are defined as follows.

$$GMD = \ln |x_1 - x_2| = \ln (w) - 1.5 \quad (3.3)$$

$$AMD = |x_1 + x_2| = \frac{w}{3} \quad (3.4)$$

$$AMSD^2 = (x_1 + x_2)^2 = (x_1 - x_2)^2 = \frac{w^2}{6} \quad (3.5)$$

Substituting the values of equation (3.3), (3.4) and (3.5) in the previously derived equation, the self-inductance is computed as the mutual inductance between all such lines (previously defined as a pair of two straight lines  $l_1$  and  $l_2$ ). The averaging technique covers the entire trapezoid and the self-inductance of such a shape is given by.

$$\begin{aligned} L &\approx \frac{\mu l}{2\pi} \left[ \ln \left( \frac{2l}{w} \right) + \frac{w}{3l} (\sqrt{2} - \ln(1 + \sqrt{2})) + \frac{w^2}{24l^2} + 0.5 \right] \\ &\approx \frac{\mu l}{2\pi} \left[ \ln \left( \frac{2l}{w} \right) + \frac{0.178w}{l} + \frac{0.047w^2}{l^2} + 0.5 \right] \end{aligned} \quad (3.6)$$

Here, the approximation covers all such pairs of lines that is present across the entire conductor sheet. When such pairs of lines are considered, the entire sheet is covered and the mutual inductance between all such lines will be summed together and form the self-inductance of the entire sheet. Thus, equation (3.6) gives the approximated equation of self-inductance for a trapezoid current sheet.

We also extend this concept to a pair of trapezoid current sheets. This is as shown in figure 3.7 where the two parallel trapezoidal sheets carry opposite current. The same techniques will be considered to compute the mutual inductance that is present between the two parallel sheets.

### 3.2.3 Mutual inductance of two parallel trapezoidal sheets

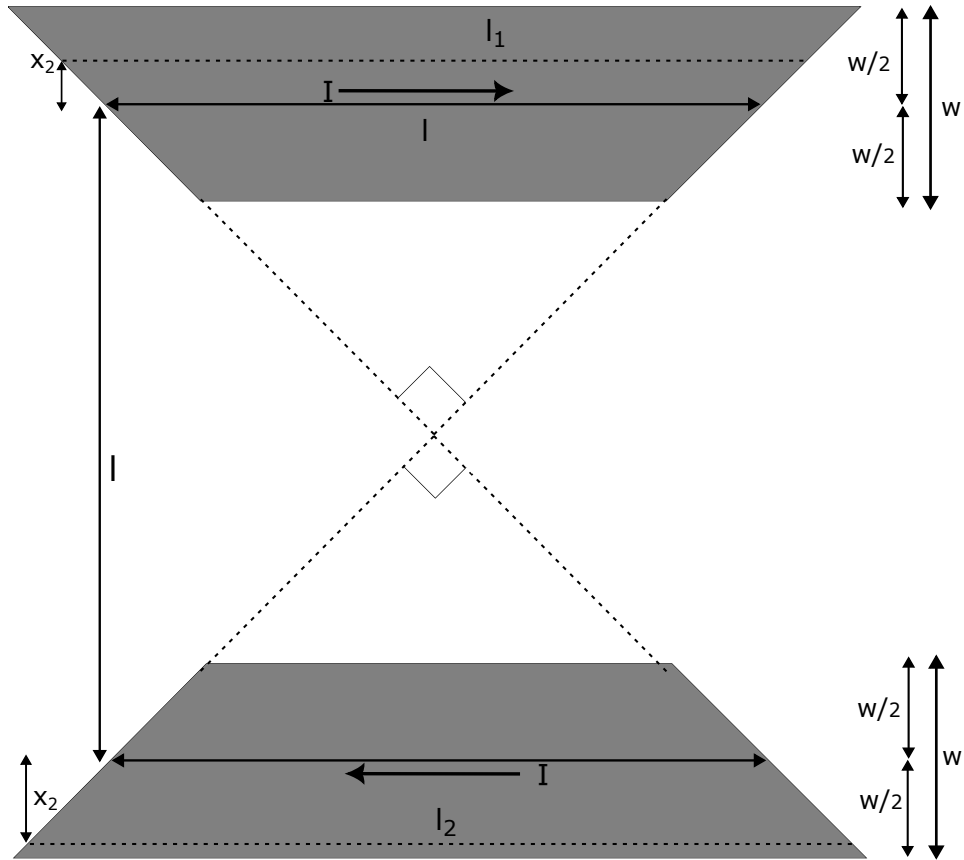


Figure 3.7: Parallel trapezoidal current sheet

An equation for mutual inductance between two parallel trapezoidal current sheets is also derived in this section. The two sheets are as shown in figure 3.7 and are separated by distance  $l$  from center to center. Here, the distances are defined similarly to the previous case of a single trapezoidal sheet. So,  $l_1 = l + 2x_1$ ,  $l_2 = l + 2x_2$  and  $R = l + x_1 + x_2$ . Again using equation 3.2, the mutual inductance between  $l_1$  and  $l_2$  is derived.

Here,

$$M = \frac{\mu}{2\pi} \left[ \left( \frac{l_1 + l_2}{2} \right) \ln \left( \sqrt{\left( \frac{l_1 + l_2}{2R} \right)^2 + 1} + \left( \frac{l_1 + l_2}{2} \right) \right) - \sqrt{\left( \frac{l_1 + l_2}{2} \right)^2 + R^2} \right] \\ - \frac{\mu}{2\pi} \left[ \left( \frac{l_1 - l_2}{2} \right) \ln \left( \sqrt{\left( \frac{l_1 - l_2}{2R} \right)^2 + 1} + \left( \frac{l_1 - l_2}{2} \right) \right) - \sqrt{\left( \frac{l_1 - l_2}{2} \right)^2 + R^2} \right]$$

Substituting the values,

$$M = \frac{\mu}{2\pi} \left[ R \left( \ln(\sqrt{2} + 1) - \sqrt{2} \right) \right] - \frac{\mu}{2\pi} \left[ (x_1 - x_2) \ln \left( \sqrt{\left( \frac{x_1 - x_2}{R} \right)^2 + 1} + \frac{(x_1 - x_2)}{R} \right) - \sqrt{(x_1 - x_2)^2 + R^2} \right]$$

$$M = \frac{\mu}{2\pi} \left[ R \left( \ln(\sqrt{2} + 1) - \sqrt{2} \right) \right] - \frac{\mu}{2\pi} \left[ (x_1 - x_2) \ln \left( 1 + \frac{1}{2} \left( \frac{x_1 - x_2}{R} \right)^2 + \frac{(x_1 - x_2)}{R} \right) - R \sqrt{1 + \left( \frac{x_1 - x_2}{R} \right)^2} \right]$$

$$M = \frac{\mu}{2\pi} \left[ R \left( \ln(\sqrt{2} + 1) - \sqrt{2} \right) \right] - \frac{\mu}{2\pi} \left[ (x_1 - x_2) \left( \frac{1}{2} \left( \frac{x_1 - x_2}{R} \right)^2 + \frac{(x_1 - x_2)}{R} \right) - R \left( 1 + \frac{1}{2} \left( \frac{x_1 - x_2}{R} \right)^2 \right) \right]$$

$$M = \frac{\mu}{2\pi} \left[ R \left( \ln(\sqrt{2} + 1) - \sqrt{2} \right) \right] - \frac{\mu}{2\pi} \left[ (x_1 - x_2) \left( \frac{1}{2} \left( \frac{x_1 - x_2}{R} \right)^2 + \frac{(x_1 - x_2)}{R} \right) - R \left( 1 + \frac{1}{2} \left( \frac{x_1 - x_2}{R} \right)^2 \right) \right]$$

$$\begin{aligned} M &= \frac{\mu}{2\pi} \left[ R \left( \ln(\sqrt{2} + 1) - \sqrt{2} \right) \right] - \frac{\mu}{2\pi} \left[ \frac{1}{2} \frac{(x_1 - x_2)^3}{R^2} + \frac{1}{2} \frac{(x_1 - x_2)^2}{R} - R \right] \\ &= \frac{\mu}{2\pi} \left[ (l + x_1 + x_2) \left( \ln(\sqrt{2} + 1) - \sqrt{2} + 1 \right) - \frac{1}{2} \frac{(x_1 - x_2)^2}{(l + x_1 + x_2)} \right] \\ &= \frac{\mu}{2\pi} \left[ (x_1 + x_2) \left( \ln(\sqrt{2} + 1) - \sqrt{2} + 1 \right) + l \left( \ln(\sqrt{2} + 1) - \sqrt{2} \right) - \frac{1}{2} \frac{(x_1 - x_2)^2}{(l + x_1 + x_2)} \right] \\ &= \frac{\mu l}{2\pi} \left[ \left( (x_1 + x_2) \left( \ln(\sqrt{2} + 1) - \sqrt{2} + 1 \right) + \left( \ln(\sqrt{2} + 1) - \sqrt{2} + 1 \right) - \frac{(x_1 - x_2)^2}{2l^2} \right) \right] \end{aligned}$$

Substituting the values for GMD, AMD and ASMD the approximated equation for the mutual inductance is,

$$M = \frac{\mu l}{2\pi} \left[ \ln(1 + \sqrt{2}) + 1 - \sqrt{2} - \frac{w^2}{12l^2} \right] \quad (3.7)$$

### 3.2.4 Approximation for a family of trapezoid sheets

The concept of current sheet can also extended to the full spiral of an on-chip inductor. The visual representation of this is shown in the following figures. The square spiral in figure 3.8 can be approximated as concentric squares and can be visualized as four trapezoidal current sheets as shown in figure 3.9.

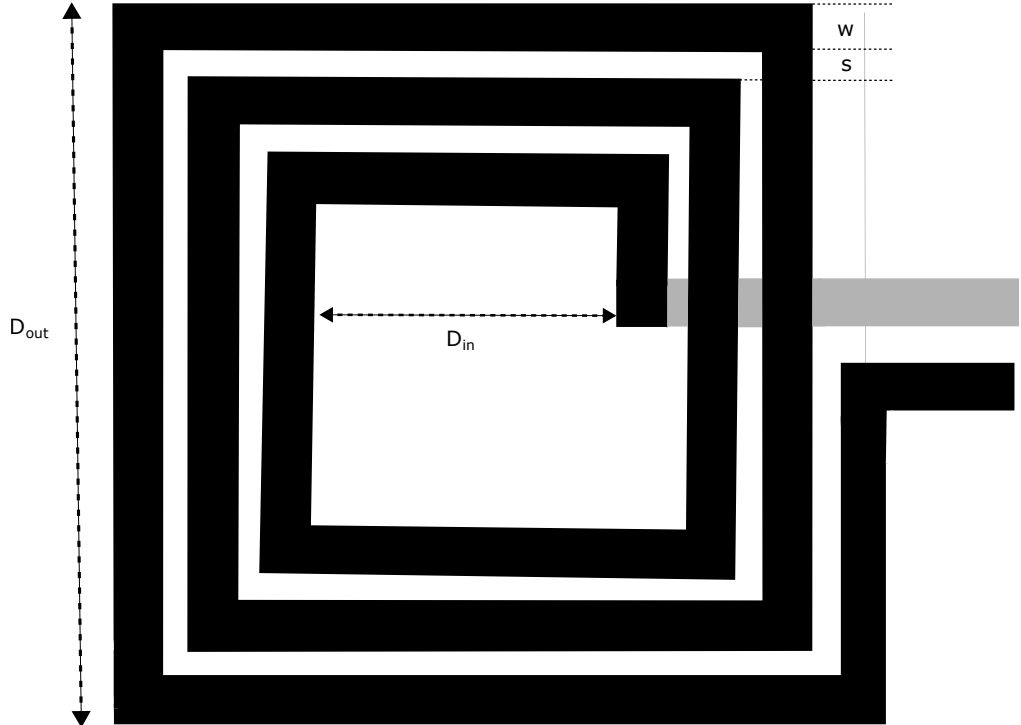


Figure 3.8: A square spiral inductor

Here,  $n$  concentric circles are approximated into four current sheets and a ratio of the filled metal and the unfilled spaces is defined as the fill ratio  $\rho$ . The same can be seen in figure 3.9 and  $\rho$  is defined as,  $\rho l = nw + (n - 1)s$ . This definition of  $\rho$  can be substituted for the width of the trapezoid.

Thus, the equation of self-inductance in equation (3.6) is modified as,

$$L_{\text{squaresheet}} = \frac{\mu n^2 l}{2\pi} \left[ \ln \left( \frac{2}{\rho} \right) + 0.178\rho + 0.5 + 0.0416\rho^2 \right] \quad (3.8)$$

Similarly, the equation for mutual inductance between two trapezoids is modified for two systems of trapezoids.

$$M_{\text{squaresheet}} = \frac{\mu n^2 l}{2\pi} [0.467 + 0.083\rho^2] \quad (3.9)$$

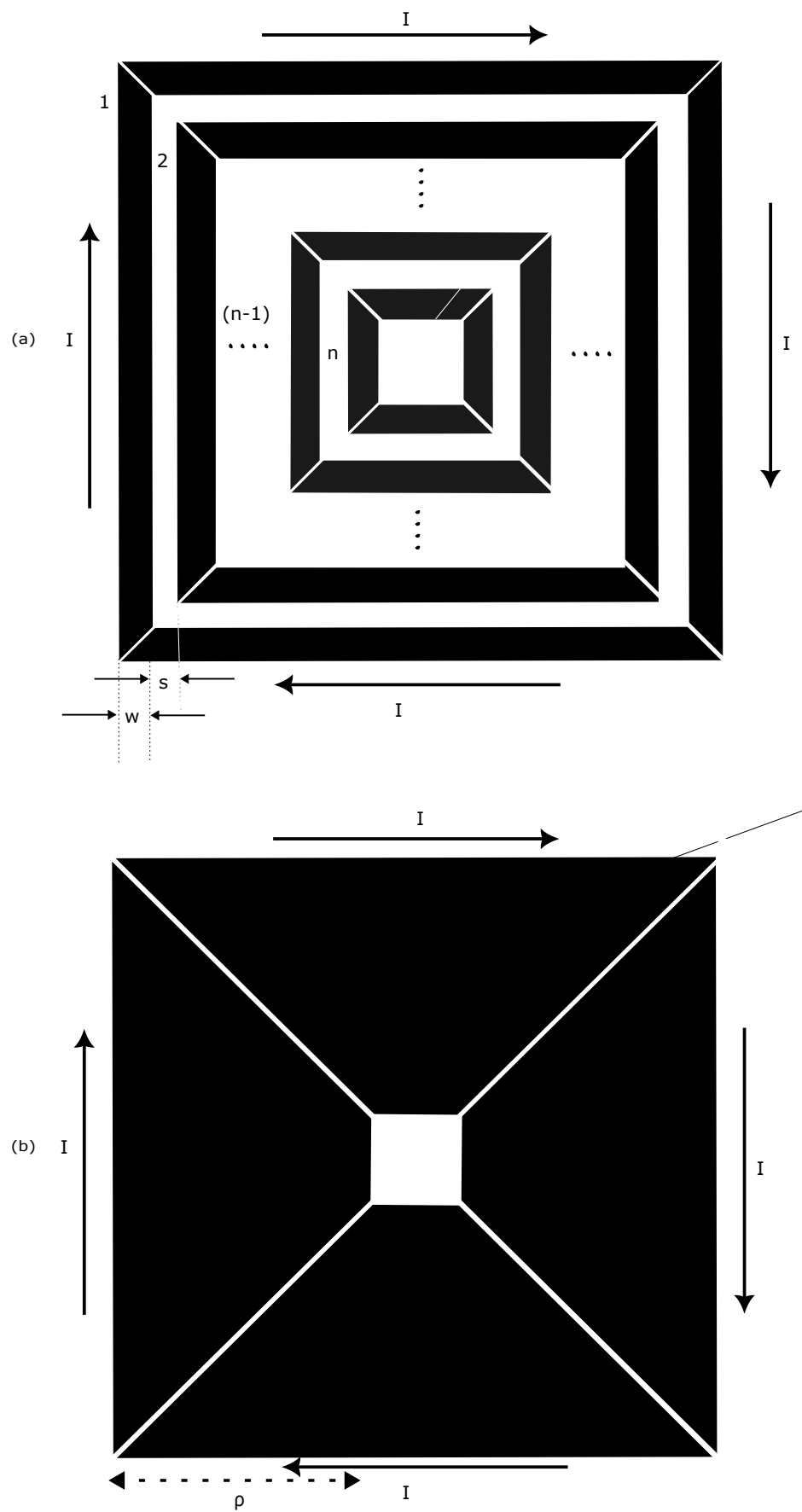


Figure 3.9: (a) Concentric squares and (b) approximated trapezoids

### 3.3 Modeling of inductor

Since inductors are built with metal strips laid on top of a substrate, parasitic effects arise due to their interaction with the substrate. Also, a series of metal resistances is present in the inductor itself. These effects of resistances and substrate capacitive interaction lower the quality of the inductor thus limiting the usage of the full inductor capability. To capture the parasitic effects in its physical form, different models as seen from [7] to [13] have been developed. One such model is given in figure 3.10

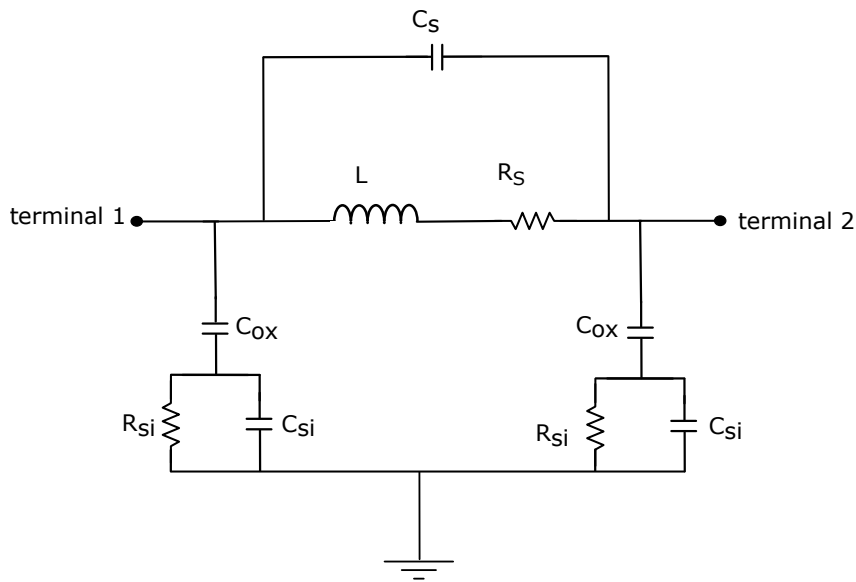


Figure 3.10: Lumped/Pi model of inductor

Here, in the Pi model,

- L is the total inductance at dc which was previously derived.
- $R_s$  is the total resistance present along with the metal and is given by,

$$R_s = \frac{\rho \cdot l}{w \cdot \delta \cdot (1 - e^{-\frac{t}{\delta}})} \quad (3.10)$$

where the resistivity of the material is  $\rho$ , the total length of the inductor is  $l$ , the width of the inductor is  $w$ , and  $\delta = \sqrt{\frac{1}{\pi f \frac{\rho}{\mu}}}$  represents the skin effect of the metal at a given frequency.

- $C_s$  is mainly contributed by the underpass and is the capacitance present between the spiral metal and the underpass.

$$C_s = n \cdot w^2 \cdot \frac{\epsilon_{ox}}{t'_{ox}} \quad (3.11)$$

here,  $t'_{\text{ox}}$  is the thickness of the oxide between the spiral metal and the underpass metal.

- $C_{\text{ox}}$  is the capacitance between the substrate and the spiral metal.

$$C_{\text{ox}} = \frac{1}{2} \cdot l \cdot w \cdot \frac{\epsilon_{\text{ox}}}{t_{\text{ox}}} \quad (3.12)$$

$t_{\text{ox}}$  is the thickness of oxide between the spiral metal and the substrate.

- $C_{\text{si}}$  is the substrate capacitance and  $R_{\text{si}}$  is the substrate resistance.

$$C_{\text{si}} = \frac{1}{2} \cdot l \cdot w \cdot C_{\text{sub}} \quad (3.13)$$

$$R_{\text{si}} = \frac{2}{l \cdot w \cdot G_{\text{sub}}} \quad (3.14)$$

Here  $G_{\text{sub}}$  and  $C_{\text{sub}}$  are the substrate conductance and substrate resistance per unit area and are treated as fitting parameters.

### 3.3.1 Derivation of series resistance

Series resistance is the resistance of the metal present inherently along with the metal trace of the inductor. This accounts for the lossy part of the inductor thereby decreasing the Quality factor. At higher frequencies, current signals tend to flow near the outer wall (as seen in figure 3.11) of the metal, and thus the current concentrates near the wall. This is because electromagnetic fields need some time to penetrate the conductor. Since inductors are generally employed in high-frequency circuits like an LC-VCO, the high frequency effect further increases the series resistance. This effect is called the 'skin effect' and it further decreases the effective conductor thickness. Resistance of a wire is defined as,

$$R = \frac{\rho \cdot l}{A}$$

where  $A$  is the area of the conductor's cross-sectional area and  $l$  is the total length of the wire. In the case of an inductor strip, we define the resistance as,

$$R_s = \frac{\rho \cdot l}{t \cdot w}$$

where  $t$  is the thickness and  $w$  is the width of the metal trace. Further,  $t$  is replaced by the total skin length  $\delta^*$  to account for the reduction of conductor area at high frequency.

$$R_s = \frac{\rho \cdot l}{\delta^* w}$$

We also define  $\delta = \sqrt{\frac{1}{\pi f \frac{\rho}{\mu}}}$  which is the skin depth for a metal whose thickness is very high as compared to the skin length.

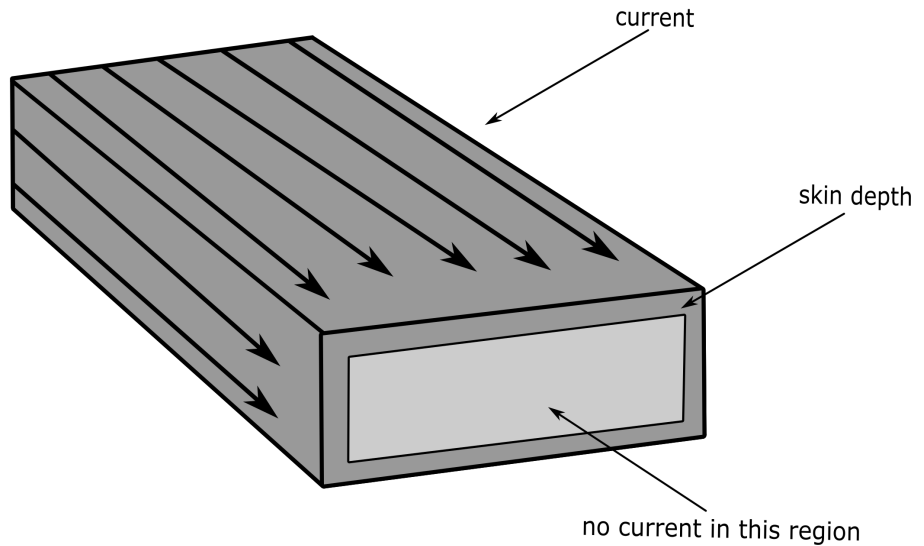


Figure 3.11: A 3-D view of a wire strip with visible skin effect

The effective skin length as given in [1] is,  $\delta^* = \delta(1 - e^{-\frac{t}{\delta}})$  and thus, the series resistance is given by,

$$R_s = \frac{\rho}{\delta(1 - e^{-\frac{t}{\delta}})} \cdot \frac{l}{w} \quad (3.15)$$

### 3.4 Quality factor of inductor

The quality factor is one of the most indispensable attributes of an inductor. The Quality factor determine how effectively the inductor can store energy in the intended form, i.e., a magnetic field. If the inductor dissipates energy in other forms of energy, the quality factor decreases. Q factor is defined as,

$$Q = 2\pi \times \frac{\text{energy stored}}{\text{energy dissipated in one cycle of oscillation}}$$

Energy stored in a pure inductor is in the form of a magnetic field. Unfortunately, other energies stored in the form of electrical energy become an unwanted component of the total energy. Thus, the quality factor expression is,

$$Q = 2\pi \times \frac{\text{peak magnetic energy} - \text{peak electrical energy}}{\text{total power loss}} \quad (3.16)$$

Modifying figure 3.10 by grounding terminal 2 and simplifying all capacitances and resistances the result is figure 3.12

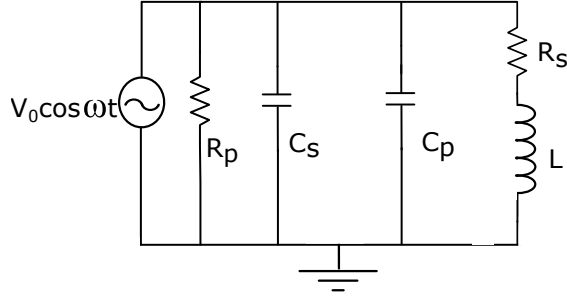


Figure 3.12: Modified form of the inductor model in figure 3.10

Here, the peak electrical energy is the total power loss in the capacitors (both  $C_p$  and  $C_s$ ) and is given by,

$$E_{E,peak} = \frac{V_0^2 C_o}{2}$$

where,  $C_o = C_p + C_s$  The peak magnetic energy is the total power of the pure inductor and is calculated to be,

$$E_{M,peak} = \frac{V_0^2 L}{2 \times [(\omega L)^2 + R_s^2]}$$

The total energy loss in one cycle is,

$$E_{loss} = \frac{2\pi}{\omega} \cdot \frac{V_0^2}{2} \cdot \left[ \frac{1}{R_p} + \frac{R_s}{(\omega L)^2 + R_s^2} \right]$$

Substituting the peak values of magnetic energy and electrical and total loss in one cycle in the equation of quality factor from equation (3.16) we have,

$$Q = \frac{\omega L}{R_s} \times \frac{R_p}{R_p + \left[ \left( \frac{\omega L}{R_s} \right)^2 + 1 \right] \cdot R_s} \times \left[ 1 - \frac{R_s^2 C_o}{L} - \omega^2 L C_o \right] \quad (3.17)$$

where,

$\frac{\omega L}{R_s}$ , gives the energy stored in pure magnetic form and the ohmic loss due to the series resistance

$\frac{R_p}{R_p + \left[ \left( \frac{\omega L}{R_s} \right)^2 + 1 \right] \cdot R_s}$ , represents the total substrate loss

$1 - \frac{R_s^2 C_o}{L} - \omega^2 L C_o$ , known as the self-resonance factor and account for the decreasing of Q with SRF

The theoretical calculations that have been done in this chapter will be verified through simulations in the proceeding chapter. Chapter 4 contains various results of simulations after implementing the inductor designed in Chapter 3 in a VCO based on complimentary operation.

# Chapter 4

## Theoretical verification and simulation results

In this chapter, a deeper analysis of the circuit performance is shown by considering the square-shaped inductor design and its performance with other circuit elements through simulations in Cadence Virtuoso. A complimentary LC-VCO setup is also considered to test various parameters of the inductor and also the overall VCO performance.

### 4.1 Theoretical calculation of the inductor under consideration

The total inductance offered by a square-shaped inductor is approximated by (3.8) and (3.9) with the former being self-inductance and the latter mutual inductance. The total inductance therefore is given by the sum of mutual inductance and the self inductance.

$$L_{\text{total}} = L_{\text{self.total}} + M_{\text{total}} \quad (4.1)$$

The mutual inductance is subtracted from the total inductance equation because the two opposite current sheets carry current in the opposite direction and contribute to negative mutual inductance. The adjacent sheets have zero mutual inductance because they are orthogonal to each other. Following the methods derived in Chapter 3, the square spiral inductor can be approximated into current sheets with four trapezoids as shown in figure 3.9. Therefore,

$$L_{\text{total}} = 4 \times L_{\text{self}} - 2 \times M \quad (4.2)$$

In this case, the inductor geometry is defined as,

Number of turns,  $n = 3$

Inner diameter,  $D_{in} = 60 \mu\text{m}$

Outer diameter,  $D_{out} = 140 \mu\text{m}$

Width of strip,  $w = 10 \mu\text{m}$

Width of spacing between two strip,  $s = 5 \mu\text{m}$

Average length of one trapezoid strip,  $l = 100 \mu\text{m}$

Fill ratio,  $\rho = 0.4$

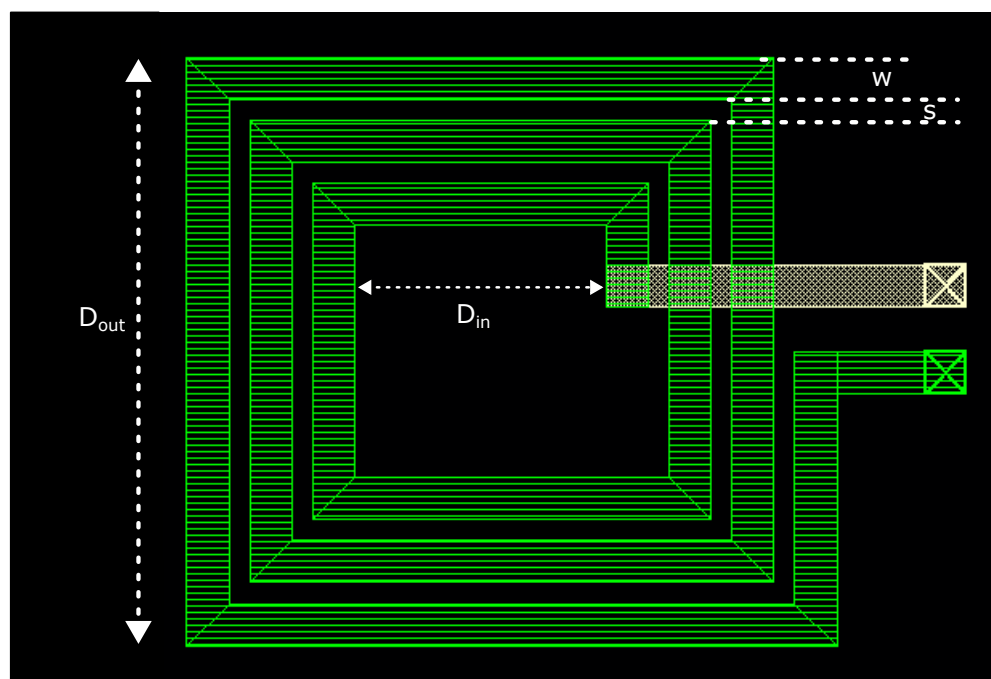


Figure 4.1: Layout view of the inductor under consideration

Using equation (3.8) the self-inductance of a single sheet is found to be,

$$L_{self} = 0.394 \text{ nH}$$

And using equation (3.9) the mutual inductance between the two opposite current sheet is found to be,

$$M = 0.0865 \text{ nH}$$

Therefore the total inductance of the inductor under consideration is,

$$\begin{aligned} L_{\text{total}} &= 4 \times 0.394 \text{ nH} + 2 \times 0.0685 \text{ nH} \\ &\approx 1.4 \text{ nH} \end{aligned}$$

#### 4.1.1 VCO implementation

The designed square inductor was implemented into a VCO architecture and to check the free-running oscillation of the oscillator, a test bench was set up with a cross-coupled complementary VCO architecture as shown in figure 4.2 to check the working of the inductor.

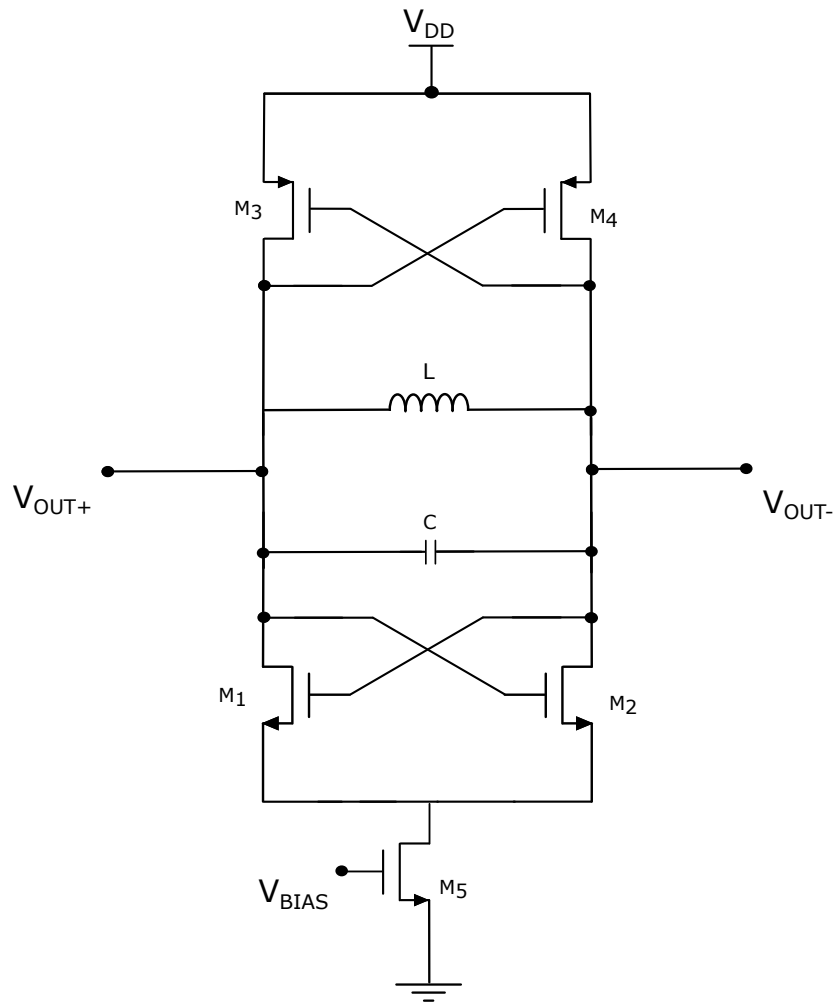


Figure 4.2: A complimentary LC-VCO circuit diagram

The layout view of the complimentary LC-VCO is shown in the following figure 4.3. The circuit was designed in TSMC 65nm technology and various layout results are also shown in the following section.

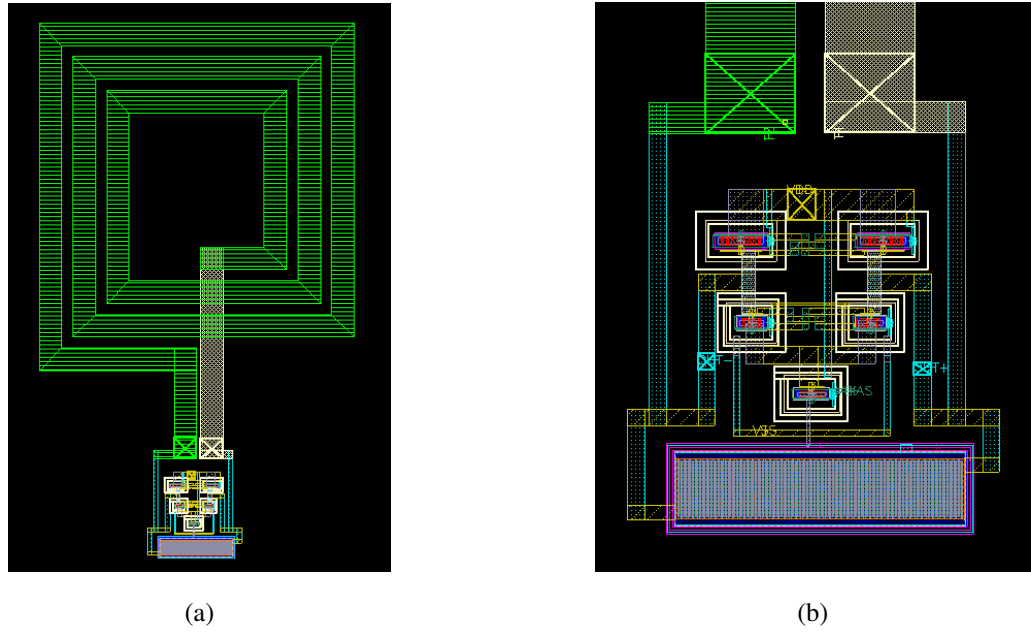


Figure 4.3: (a) Layout view of LC-VCO and (b) Zoomed-in view of the LC-VCO

## 4.2 Simulation Results

Various post-layout simulations were performed to check the working of the inductor in a full VCO environment setup. Emx simulation was also done to check the quality factor and the inductance offered by the design under consideration.

### 4.2.1 EMX simulations

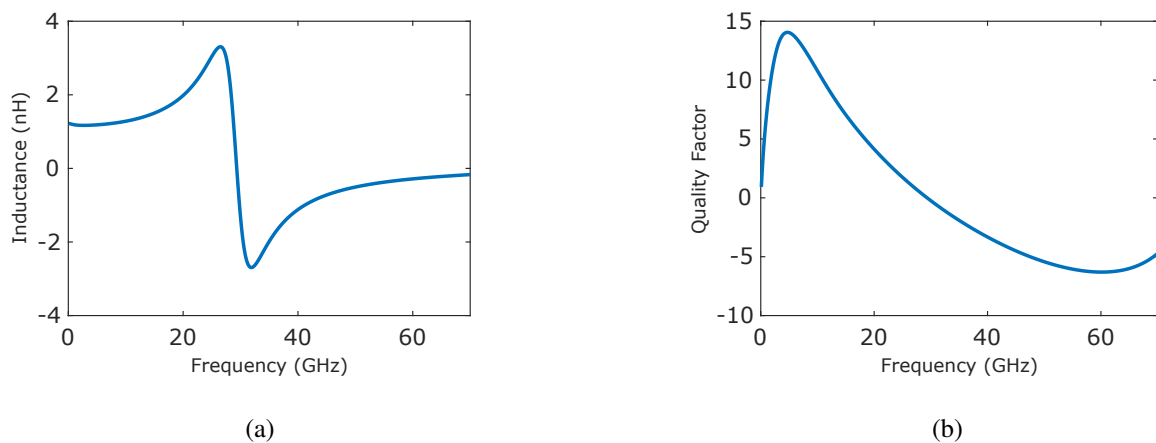


Figure 4.4: (a) Inductance vs frequency and (b) Quality factor vs frequency

#### 4.2.2 Post Layout simulation results

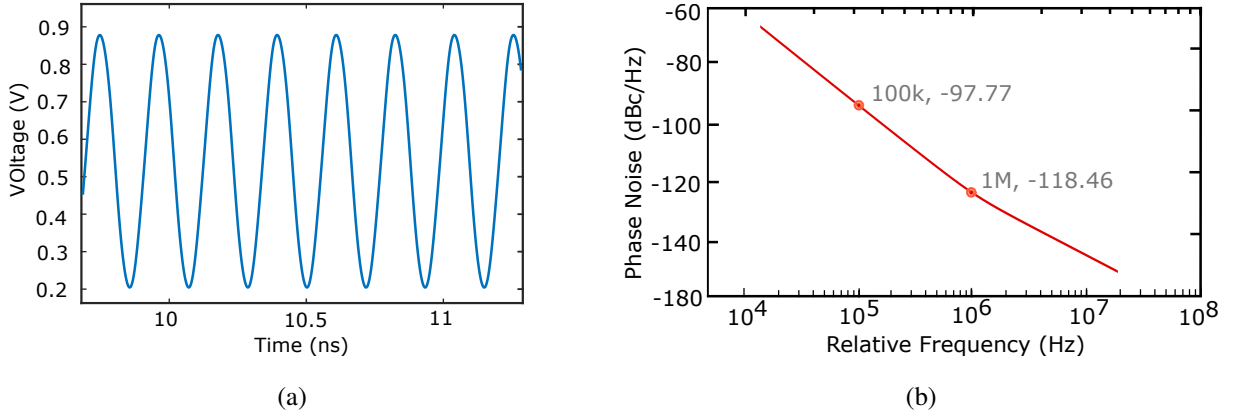


Figure 4.5: (a) Voltage swing of the LC-VCO and (b) Phase Noise of the LC-VCO

A simulation was also set up for PVT variation for all three process corners TT, FF, SS, and 27 simulations were performed to check all the process corners for supply voltage of 0.9 V, 1 V and 1.1 V and a temperature range from  $-20^{\circ}\text{C}$  to  $127^{\circ}\text{C}$ . The following figures 4.6 and 4.8d show the same for all the simulations of process corners.

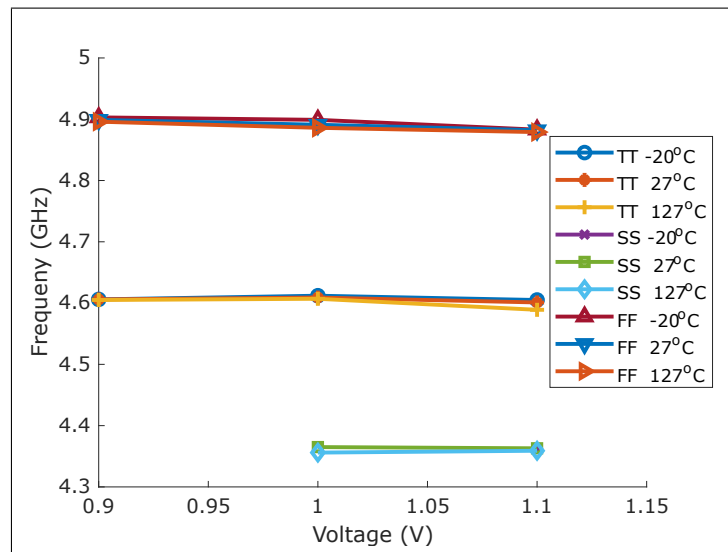


Figure 4.6: Variation of frequency for temperature change from  $-20^{\circ}\text{C}$  to  $127^{\circ}\text{C}$  and for sensitivity of supply voltage from 0.9 V to 1.1V

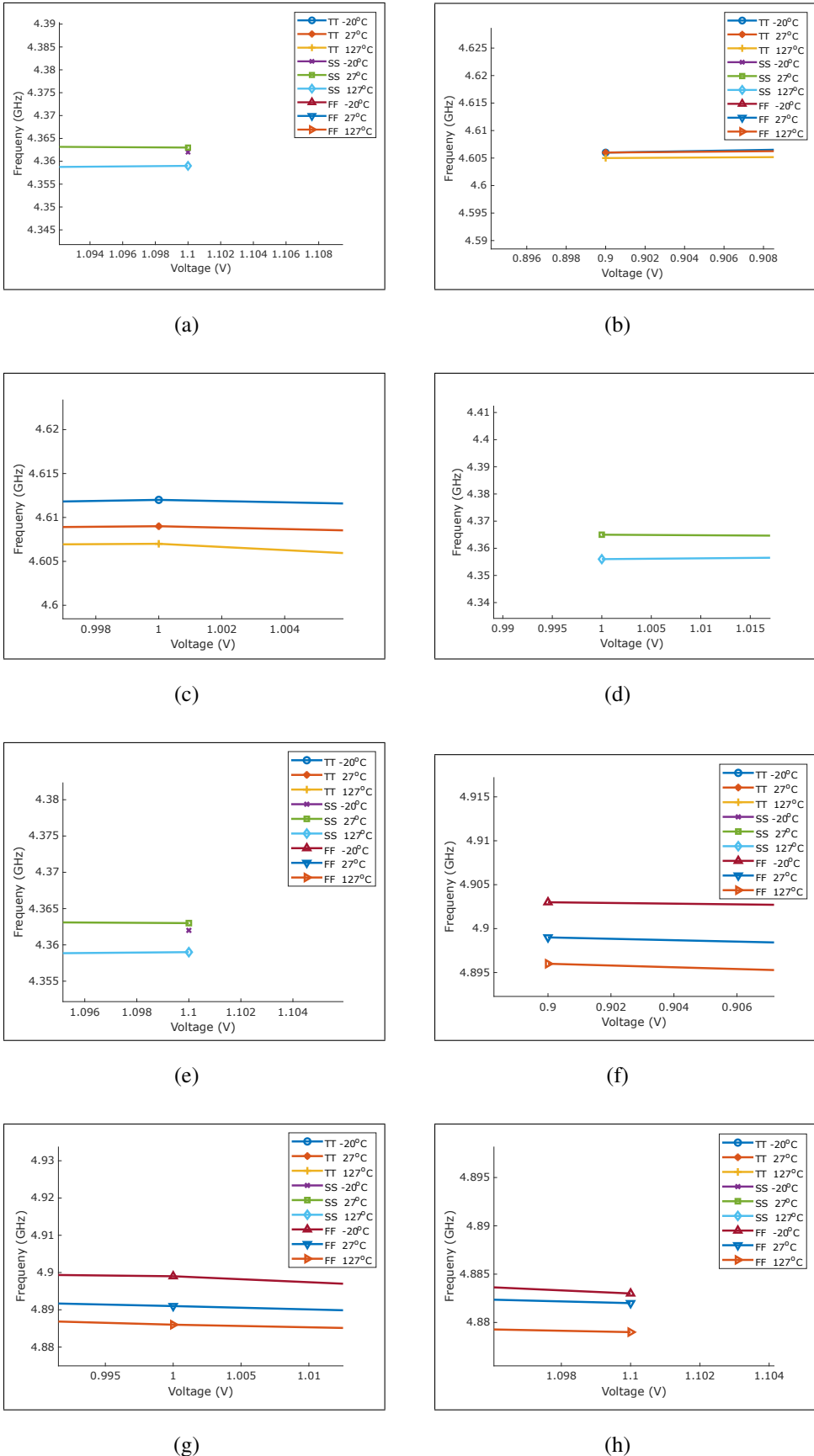


Figure 4.7: (a) to (h) shows individual points of the PVT simulations from figure 4.6

A Monte Carlo simulation for process variation and mismatch was also performed. 200 simulations were done for frequency, power consumption, and phase noise @ 100 KHz and 1 MHz.

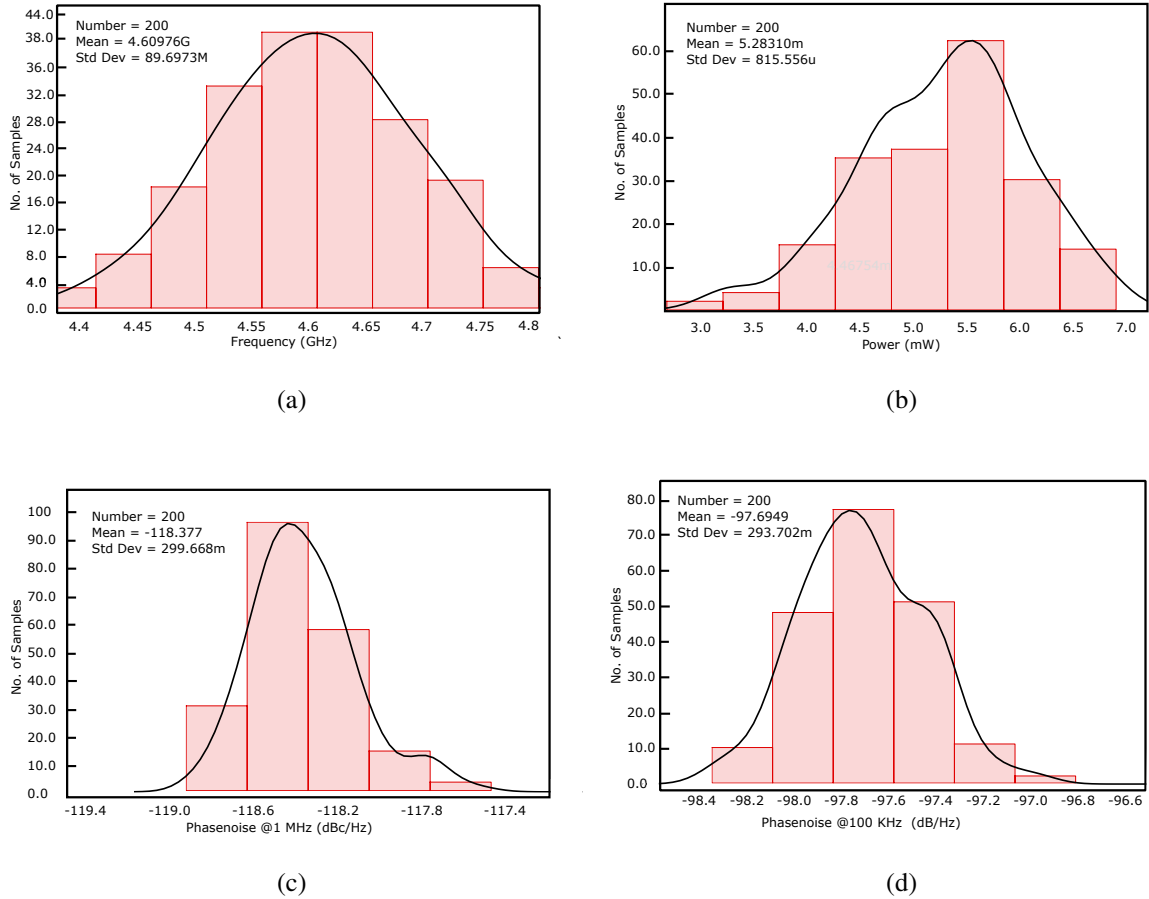


Figure 4.8: Monte Carlo simulation results for mismatch and process variation of (a) Frequency, (b) Power consumption, (c) Phase noise @ 100 KHz, and (d) Phase noise @ 1 MHz

Table 4.1: Specification of the designed LC-VCO

Parameter	Value
Voltage Swing	223.5 mV to 898 mV
Power	5.96 mW
Frequency	4.601 GHz
Phase noise @ 100K (dBc/Hz)	-97.77
Phase noise @ 1M (dBc/Hz)	-118.46
FOM @ 100K	183
FOM @ 1M	184

The figure of merit (FOM) of a VCO is given by,

$$FOM = 20\log\left(\frac{f_o}{\Delta f}\right) - PN@\Delta f - 10\log\left(\frac{\text{Power}}{1\text{mW}}\right)$$

### 4.3 Comparison

A comparison of the different formulas along with the derived formula of this work is given in the table below. The same inductor specification of Chapter 3 is used to compare the formulas.

Table 4.2: Comparison table of different formulas

Parameter	This work	[5]	Modified Wheeler [1]	Monomial fit [1]
Inductance	1.4 nH	1.76 nH	1.26 nH	1.242 nH

A comparison table for different LC-VCO architectures is given in the table below. This comparison is made in terms of technology used, frequency of operation, supply voltage, power consumption, phase noise, and figure of merit.

Table 4.3: Comparison table for different architectures of LC-VCO

Parameters	This work	TCAS22 [16]	TEC19 [19]
Technology	65 nm	65 nm	180 nm
Frequency (GHz)	4.601	29.12	2.6
Supply voltage	1 V	1 V	1.8 V
DC power	5.96 mW	16.8 mW	-
PN@1 MHz (dBc/Hz)	-118.46	-105.34	-122
FOM@1 MHz (dBc/Hz)	184	182.37	174

This concludes the analysis of the inductor, its simulations, and its performance in the VCO environment. The next part of the report contains the conclusion and other future works that are going to be continued in the next phase of the project.

# **Chapter 5**

## **Conclusion and future works**

The report presents the overview of inductance calculation based on current sheet approximation and testing the designed inductor with the help of a complementary VCO. A comparison also has been made to compare how the derived formulas compare with other working formulas. This formula can be used to predict how an inductor would behave by looking into the geometrical properties of the inductor like the width of the strip or the inner/outer diameter. Hence, a planned design with control over the inductance or the quality factor can be done prior to actual simulation or fabrication.

Since simple formulas work well only with basic structures like square-shaped or hexagonal-shaped inductors, formulas and models will be used along with simulation tools like EMX to further characterize the inductor behavior of more complex shapes. MTP phase 2 will cover the details of modeling and dive deeper into the electromagnetic behavior of inductors when complex structures are involved. And the inductor behavior in the overall control of frequency at the VCO level will also be included in the future.

# References

- [1] S. Mohan, M. del Mar Hershenson, S. Boyd, and T. Lee, “Simple accurate expressions for planar spiral inductances,” *IEEE Journal of Solid-State Circuits*, vol. 34, no. 10, pp. 1419–1424, 1999.
- [2] H. Greenhouse, “Design of planar rectangular microelectronic inductors,” *IEEE Transactions on Parts, Hybrids, and Packaging*, vol. 10, no. 2, pp. 101–109, 1974.
- [3] F. W. Grover, “Inductance calculations working formulas and tables,” *Dover Publications, Inc*, 1946.
- [4] S. Jenei, B. Nauwelaers, and S. Decoutere, “Physics-based closed-form inductance expression for compact modeling of integrated spiral inductors,” *IEEE Journal of Solid-State Circuits*, vol. 37, no. 1, pp. 77–80, 2002.
- [5] B. Razavi, “RF Microelectronics,” *Prentice Hall*, 1998.
- [6] S. Mohan, “The design, modeling and optimization of on-chip inductor and transformer circuits,” *Ph.D thesis, Stanford University*, 07 2000.
- [7] C. Yue, C. Ryu, J. Lau, T. Lee, and S. Wong, “A physical model for planar spiral inductors on silicon,” in *proceedings of International Electron Devices Meeting. Technical Digest*, pp. 155–158, 1996.
- [8] W. Kuhn, X. He, and M. Mojarradi, “Modeling spiral inductors in SOS processes,” *IEEE Transactions on Electron Devices*, vol. 51, no. 5, pp. 677–683, 2004.
- [9] J. Crols, P. Kinget, J. Craninckx, and M. Steyaert, “An analytical model of planar inductors on lowly doped silicon substrates for high-frequency analog design up to 3 GHz,” in *proceedings of Symposium on VLSI Circuits. Digest of Technical Papers*, pp. 28–29, 1996.

- [10] Y. Koutsoyannopoulos and Y. Papananos, “Systematic analysis and modeling of integrated inductors and transformers in RF IC design,” *IEEE Transactions on Circuits and Systems II: Analog and Digital Signal Processing*, vol. 47, no. 8, pp. 699–713, 2000.
- [11] Y. Tian, F. Y. Huang, Y. Wang, X. Tang, and N. Jiang, “Modeling of on-chip spiral inductors with a center-tap,” in *proceedings of 9th International Conference on Solid-State and Integrated-Circuit Technology*, pp. 500–503, 2008.
- [12] Hooman Darabi, “Radio frequency integrated circuits and systems,” *Cambridge University Press*, 2015.
- [13] J. Chen and J. Liou, “Improved and physics-based model for symmetrical spiral inductors,” *IEEE Transactions on Electron Devices*, vol. 53, no. 6, pp. 1300–1309, 2006.
- [14] M. Danesh and J. Long, “Differentially driven symmetric microstrip inductors,” *IEEE Transactions on Microwave Theory and Techniques*, vol. 50, no. 1, pp. 332–341, 2002.
- [15] A. Niknejad and R. Meyer, “Analysis, design, and optimization of spiral inductors and transformers for Si RF ICs,” *IEEE Journal of Solid-State Circuits*, vol. 33, no. 10, pp. 1470–1481, 1998.
- [16] T.-H. Huang, S.-F. Yang, and S.-T. Lin, “Characterization of a planar honeycomb-based inductor on crosstalk/emi suppression,” *IEEE Transactions on Electromagnetic Compatibility*, vol. 61, no. 2, pp. 504–511, 2019.
- [17] S. Tayenjam, V. N. R. Vanukuru, and S. Kumaravel, “A pcell design methodology for automatic layout generation of spiral inductor using skill script,” in *proceedings of International conference on Microelectronic Devices, Circuits and Systems (ICMDCS)*, pp. 1–4, 2017.
- [18] Gaurav Agarwal, “On-chip spiral inductor for LC-based Voltage Control Oscillator (LC-VCO),” *Master thesis , IIT Ropar*, 2024.
- [19] F. Hong, H. Zhang, and D. Zhao, “An x-band cmos vco using ultra-wideband dual common-mode resonance technique,” *IEEE Transactions on Circuits and Systems I: Regular Papers*, vol. 69, no. 9, pp. 3579–3590, 2022.